J. Fluid Mech. (1991), vol. 233, pp. 561–585
Printed in Great Britain

Asymmetric oscillations in thermosolutal convection

By D. R. MOORE[1], N. O. WEISS[2] AND J. M. WILKINS[2]
[1] Department of Mathematics, Imperial College, London SW7 2BZ, UK
[2] Department of Applied Mathematics and Theoretical Physics, University of Cambridge, Silver Street, Cambridge CB3 9EW, UK

(Received 14 September 1990 and in revised form 19 April 1991)

Thermosolutal convection provides a testbed for applications of nonlinear dynamics to fluid motion. If the ratio of solutal to thermal diffusivity is small and the solutal Rayleigh number R_S is large, instability sets in at a Hopf bifurcation as the thermal Rayleigh number R_T is increased. For two-dimensional convection in a rectangular box the fundamental mode is a single roll with point symmetry about its axis. The symmetries of periodic and steady solutions form an eighth-order group with invariant subgroups that describe pure single-roll and multiroll solutions. A systematic numerical investigation reveals a rich variety of spatiotemporal behaviour in the regime where $R_S \gg R_T - R_S > 0$. Point symmetry is broken and there is a branch of spatially asymmetric periodic solutions. These mixed-mode oscillations lose their temporal symmetry in a subsequent bifurcation, followed eventually by a transition to chaos. The numerical experiments can be interpreted by relating the physical form of the solutions to an appropriate bifurcation structure.

1. Introduction

Double convection offers examples of a wide range of dynamical behaviour in continuous fluid systems. Travelling waves, standing waves and steady motion have all been detected in laboratory experiments on convection in binary fluids and their interactions can be compared with theoretical predictions. Idealized thermosolutal convection provides the simplest model problem and the behaviour of a layer with a bottom-heavy solute concentration, destabilized by heating from below, has been studied in considerable detail. In the absence of motion the density gradient is proportional to the difference between the solutal Rayleigh number R_S and the thermal Rayleigh number R_T but it is possible to excite either travelling waves or periodic oscillations (depending on the lateral boundary conditions) when $R_T \ll R_S$, since the solute diffuses less rapidly than heat. When R_S, R_T are both large and $R_T \approx R_S$ there is a static solution in which the density is almost uniform. The different diffusion rates ensure, however, that any motion produces large gradients in density. Hence the dynamics in this regime is particularly rich. Earlier numerical investigations have been concerned with complicated temporal behaviour in a system constrained by imposed spatial symmetries. Here we consider bifurcations at which those symmetries are broken and follow the resulting branches of mixed-mode solutions.

The symmetries of both steady and periodic solutions can be classified by establishing the appropriate group structure. McKenzie (1988) has discussed bifurcations involving symmetry changes in some detail, emphasizing temporal as well as spatial symmetries. His systematic treatment exploits the formalism developed by crystallographers to study periodic lattices. This general method is particularly effective in describing planform changes in three-dimensional convection. We shall, however, be concerned with a two-dimensional configuration, where the symmetries are simpler to describe. This idealized problem allows us to develop an explicit treatment of the symmetries of the system and of its solutions. The appropriate eighth-order symmetry group contains the symmetries of pure steady and periodic solutions as invariant subgroups. These symmetries may be broken in secondary bifurcations leading to branches of mixed-mode solutions, whose remaining symmetries can be predicted.

The value of this general approach is demonstrated by applying it to a numerical study of symmetry breaking in the nonlinear regime. We consider convection in the rectangular region $\{0 \leqslant x \leqslant \lambda;\ 0 < z < 1\}$ with mirror symmetry about the lateral boundaries. In most previous numerical experiments point symmetry was imposed about the roll-axis at $x/\lambda = z = \frac{1}{2}$. Thus the stream function Ψ, the temperature fluctuation Θ and the fluctuation in solute concentration Σ possessed the symmetry

$$(x, z) \rightarrow (\lambda - x, 1 - z), \quad (\Psi, \Theta, \Sigma) \rightarrow (\Psi, -\Theta, -\Sigma). \tag{1}$$

This is the symmetry of the fundamental eigenfunction of the linear problem, with a single roll in the domain. We shall investigate behaviour when the constraint (1) is relaxed. Although the oscillatory solutions are initially point-symmetric we find that as R_T is increased there is a bifurcation at which the symmetry (1) is broken. The branch of spatially asymmetric solutions can then be followed until it approaches a heteroclinic bifurcation. Some preliminary results have been reviewed elsewhere (Moore & Weiss 1990; Weiss 1990). Similar behaviour has been found for two-dimensional magnetoconvection (Weiss 1981; Proctor & Weiss 1982), where the bifurcation structure can be related to a seventeenth-order model system (Nagata, Proctor & Weiss 1990). This model confirms that asymmetric oscillations correspond to mixed-mode solutions on solution branches that bifurcate from the branches with symmetric single-roll or two-roll solutions in the region. Physically, narrow solutal plumes combine with broader thermal plumes to produce complicated density distributions which dominate the motion.

The transition from spatially symmetric to asymmetric periodic oscillations is obscured by the appearance of temporal chaos. Huppert & Moore (1976) discovered aperiodic behaviour for solutions with imposed point symmetry and an aspect ratio $\lambda = \surd 2$. Subsequently Moore *et al.* (1983) and Knobloch *et al.* (1986*b*), using the same finite-difference code with $R_S = 10^4$ and a mesh interval $\Delta x = \lambda/N_x$, $N_x = 12$ found that there was a bubble of chaos contained between two cascades of period-doubling bifurcations and followed by more complicated time-dependent behaviour; they also used a different code to investigate behaviour with $\lambda = 1.5$ and $N_x = 24$, and established the existence of several bubbles towards the end of the oscillatory branch. This bifurcation structure corresponded to that found in low-order model systems where chaos is caused by a heteroclinic bifurcation with eigenvalues that satisfy Shil'nikov's criterion (Guckenheimer & Holmes 1983; Wiggins 1988). Indeed, it has since been shown analytically that the Shil'nikov mechanism leads to chaos in the partial differential equations in a particular asymptotic limit as $\lambda \rightarrow 0$ (Proctor & Weiss 1990). As more powerful computing facilities became available the numerical experiments were repeated at much higher resolution. Shi & Orszag (1987), using spectral methods, showed that for $\lambda = \surd 2$ the first bubble got no further than the first period-doubling bifurcation; this has been confirmed by us and we have also demonstrated that the complete cascade just survives with $\lambda = 1.5$ (Moore, Weiss & Wilkins 1990*b*). The bifurcation structure is apparently robust but sensitive to changes in all parameters, so that chaos appears in this bubble if either the physical parameter R_T or the geometrical parameter λ or the discretization parameter Δx is increased. Although Shi & Orszag (1987) found examples of solutions with period two and period three they claimed that with sufficiently high resolution all solutions on the oscillatory branch were periodic. They also asserted that chaotic behaviour was a result of insufficient resolution (Goldhirsch, Pelz & Orszag 1989). We have, however, succeeded in showing that the transition to chaos for $\lambda = 1.4$ as $\Delta x \to 0$ is consistent with the bifurcation sequence in quadratic maps, as expected for the Shil'nikov mechanism (Moore *et al.* 1990*b*). Shi & Orszag were correct in emphasizing the importance of ensuring adequate resolution but failed to recognize the underlying bifurcation structure; so they misinterpreted their own results.

The advantage of numerical experiments is that specific bifurcations can be located and identified. Care and experience are, however, needed in order to interpret the results correctly. All bifurcations are affected by discretization. Even if the bifurcation structure is robust the bifurcation sets will be shifted in parameter space. In addition, truncation may introduce extra bifurcations that are not present in the partial differential equations, owing to lack of spatial or temporal resolution. These two situations can be distinguished by introducing extra parameters (e.g. the mesh interval and timestep) to represent discretization and then establishing the bifurcation structure in the limit as those parameters tend consistently to zero (Moore *et al.* 1990*b*). To achieve this it is necessary to understand both the effects of numerical errors and the underlying bifurcation structure of the problem.

In the next section we outline our model problem and establish the group structure that describes the symmetries of the system and of its solutions. The behaviour of solutions with point symmetry is discussed in §3. Next, in §4, we locate the symmetry-breaking bifurcation and describe mixed-mode periodic solutions. The branches of mixed-mode oscillatory solutions are followed through saddle-node and period-doubling bifurcations to chaos in §5. Then, in §6, the bifurcation structure is discussed and related to normal form equations. In the final section we assess the significance of these results and their application to a wider class of problems.

2. Symmetries of the model problem

Two-dimensional thermosolutal convection in a Boussinesq fluid is described by the non-dimensional equations

$$\partial_t \omega + \partial(\Psi, \omega) = \sigma[R_S \partial_x \Sigma - R_T \partial_x \Theta + \nabla^2 \omega], \tag{2}$$

$$\partial_t \Theta + \partial(\Psi, \Theta) = \partial_x \Psi + \nabla^2 \Theta, \tag{3}$$

$$\partial_t \Sigma + \partial(\Psi, \Sigma) = \partial_x \Psi + \tau \nabla^2 \Sigma, \tag{4}$$

where the vorticity

$$\omega = -\nabla^2 \Psi \tag{5}$$

(Veronis 1968; Huppert & Moore 1976; Knobloch *et al.* 1986*b*). Here the normalized temperature $T = \frac{1}{2} - z + \Theta(x, z, t)$, the normalized solute concentration $S = \frac{1}{2} - z + \Sigma(x, z, t)$ and σ, τ are the ratios of the viscous and solutal diffusivities respectively to the thermal diffusivity. We impose reflection symmetry about the lateral boundaries and adopt idealized (stress-free) boundary conditions so that

$$\Psi = \partial_z^2 \Psi = \Theta = \Sigma = 0 \quad \text{on} \quad z = 0, 1, \tag{6}$$

$$\Psi = \partial_x^2 \Psi = \partial_x \Theta = \partial_x \Sigma = 0 \quad \text{on} \quad x = 0, \lambda. \tag{7}$$

The system (2)–(7) depends on five dimensionless parameters, four physical (R_S, R_T, σ, τ) and one geometrical (λ).

This system has three important symmetries. The first, m_x, corresponds to reflection in the vertical plane $x = \frac{1}{2}\lambda$ (left–right symmetry) so that

$$(x,z) \to (\lambda - x, z), \quad (\Psi, \Theta, \Sigma) \to (-\Psi, \Theta, \Sigma). \tag{8}$$

The second, m_z, corresponds to reflection in the horizontal plane $z = \frac{1}{2}$ (up–down symmetry) so that

$$(x,z) \to (x, 1-z), \quad (\Psi, \Theta, \Sigma) \to (-\Psi, -\Theta, -\Sigma). \tag{9}$$

The third, $i = m_x m_z$, is the point symmetry (1). Thus the system (2)–(7) has the spatial symmetry of a rectangle, corresponding to the fourth–order dihedral group D_2 (Nagata *et al.* 1990). In addition, it has a symmetry with respect to arbitrary displacements of the origin in time ($t \to t+p, p \in \Re$), corresponding to a Lie group $\mathscr{T}$. The full symmetry group is therefore $D_2 \otimes \mathscr{T}$.

Any solution can be expanded in Fourier series as

$$\Psi(x,z,t) = \sum_m \sum_n a_{mn}(t) \sin(m\pi x/\lambda) \sin n\pi z, \tag{10}$$

$$\Theta(x,z,t) = \sum_m \sum_n b_{mn}(t) \cos(m\pi x/\lambda) \sin n\pi z, \tag{11}$$

$$\Sigma(x,z,t) = \sum_m \sum_n d_{mn}(t) \cos(m\pi x/\lambda) \sin n\pi z. \tag{12}$$

Solutions may be invariant under one or more spatial symmetries. A solution that is invariant under m_x has m even in (10)–(12); the fundamental solution with this symmetry has two rolls in the domain and $a_{21} \neq 0$. A solution invariant under m_z has n even; the fundamental solution has two stacked rolls and $a_{12} \neq 0$. Solutions with point symmetry are invariant under i and have $(m+n)$ even in (10)–(12); the fundamental has $a_{11} \neq 0$. Solutions with both m and n even have the full D_2 symmetry; the fundamental has four rolls and $a_{22} \neq 0$. There are also infinitely many other multiroll solutions. It can easily be verified that these symmetries are preserved as the solutions evolve in time.

Now the system (2)–(7) possesses a trivial static solution $\Psi = \Theta = \Sigma = 0$ for all values of the parameters. For $\tau < 1$ and $R_S > R_S^{(c)} \equiv R_0 \tau^2(1+\sigma)/[\sigma(1-\tau)]$, where $R_0 = \pi^4(1+\lambda^2)^3/\lambda^4$ is the critical Rayleigh number when $R_S = 0$, convection sets in at an oscillatory (Hopf) bifurcation when $R_T = R_T^{(o)}$ and this is followed by a stationary bifurcation at $R_T = R_T^{(e)} > R_T^{(o)}$. We shall adopt standard values for the parameters and restrict our attention to behaviour with $\sigma = 1$, $\tau = 10^{-\frac{1}{2}}$, $R_S = 10^4$ and $\lambda = 1.5$. Thus we are only free to vary the selected parameter R_T. Then the first mode to become unstable is a single roll with point symmetry i, followed by two rolls with mirror symmetry m_x. Values of $R_T^{(o)}$ and $R_T^{(e)}$ for modes with different symmetries are listed in table 1. Note that the bifurcations for the single-roll and two-roll solutions occur close together, since $R_S \gg R_0$, and that the stacked rolls only appear at much higher values of R_T.

In what follows we shall only be concerned with interactions between single-roll, two-roll and stacked-roll solutions, with symmetries i, m_x and m_z respectively. It is first necessary to establish the appropriate symmetry group for this problem. McKenzie (1988) has outlined a systematic procedure based on the formalism

	Single-roll	Two-roll	Two stacked rolls	Four rolls
Symmetry	i	m_x	m_z	D_2
(m, n)	(1, 1)	(2, 1)	(1, 2)	(2, 2)
$R_T^{(o)}$	7725	8616	39916	24890
$R_T^{(e)}$	32283	32797	50864	42191

TABLE 1. Bifurcation values for $R_S = 10^4$, $\lambda = 1.5$, $\tau = 10^{-\frac{1}{2}}$ and $\sigma = 1$

developed for crystallography but our simple two-dimensional problem allows an explicit description of the symmetries of steady and periodic solutions which demonstrates the power of this approach.

We begin by considering bifurcations involving steady solutions only, so that all solutions retain the symmetry $\mathscr{T}$. The general theory has been discussed by Sattinger (1978) and Golubitsky & Schaeffer (1985); here we follow the treatment of the analogous problem in magnetoconvection by Nagata *et al.* (1990). The trivial solution has the full D_2 symmetry of the system, which is broken at a stationary bifurcation when $R_T = R_T^{(e)}$. Solutions on branches emerging from this primary bifurcation have Z_2 symmetry corresponding to one of i, m_x or m_z. For $R_T > R_T^{(e)}$ there are always two solutions related by the broken symmetries: hence there are only pitchfork bifurcations from the trivial solution, giving rise to two equivalent solution branches. For example, the two equivalent single-roll solutions with symmetry i correspond to rolls rotating in opposite directions, which are related by the symmetry m_x or by the symmetry $m_z = im_x$. The symmetry of pure nonlinear solutions may be broken at a secondary bifurcation, giving rise to branches of mixed-mode solutions that only possess the trivial symmetry E. These branches may provide links between branches with different symmetries but it is not possible to recognize those symmetries by inspecting the mixed-mode solutions.

We now extend this description to include periodic solutions, together with interactions between steady and periodic solutions (but excluding any quasi-periodic or aperiodic behaviour). Then the continuous symmetry $\mathscr{T}$ is broken and we regard all solutions as being periodic with some period P. To find this period we inspect solutions at times t, $t+p$ as both t and p are varied continuously. If the solution is invariant for all p over some finite interval then it is steady and we may choose P arbitrarily. If the solution repeats only at intervals $p = rP$ $(r = 1, 2, 3, \ldots)$ then we choose P as the *least* period for which repetition occurs. Next we identify $t+P$ with t so that t lies in the interval $(0, P)$ and (x, z, t) lie on a cylindrical surface $(\mathfrak{R} \times S)$. The spatial symmetries in (8), (9) and (10) can now be redefined as

$$m_x\colon \quad (x,z,t) \to (\lambda - x, z, t), \quad (\Psi, \Theta, \Sigma) \to (-\Psi, \Theta, \Sigma), \tag{13}$$

$$m_z\colon \quad (x,z,t) \to (x, 1-z, t), \quad (\Psi, \Theta, \Sigma) \to (-\Psi, -\Theta, -\Sigma), \tag{14}$$

$$i\colon \quad (x,z,t) \to (\lambda - x, 1-z, t), \quad (\Psi, \Theta, \Sigma) \to (\Psi, -\Theta, -\Sigma). \tag{15}$$

Each of these operations is its own inverse, so that

$$m_x^2 = m_z^2 = i^2 = E\colon \quad (x,z,t) \to (x,z,t), \quad (\Psi, \Theta, \Sigma) \to (\Psi, \Theta, \Sigma). \tag{16}$$

To distinguish between different solutions we inspect them after half a period. Then all steady solutions possess the symmetry

$$t_e\colon \quad (x,z,t) \to (x, z, t + \tfrac{1}{2}P), \quad (\Psi, \Theta, \Sigma) \to (\Psi, \Theta, \Sigma). \tag{17}$$

	E	m_x	m_z	i	t_x	t_z	t_i	t_e
E	E	m_x	m_z	i	t_x	t_z	t_i	t_e
m_x	m_x	E	i	m_z	t_e	t_i	t_z	t_x
m_z	m_z	i	E	m_x	t_i	t_e	t_x	t_z
i	i	m_z	m_x	E	t_z	t_x	t_e	t_i
t_x	t_x	t_e	t_i	t_z	E	i	m_z	m_x
t_z	t_z	t_i	t_e	t_x	i	E	m_x	m_z
t_i	t_i	t_z	t_x	t_e	m_z	m_x	E	i
t_e	t_e	t_x	t_z	t_i	m_x	m_z	i	E

TABLE 2. The group multiplication table for symmetries of steady and periodic solutions

Any periodic solution on a branch emerging from a primary Hopf bifurcation reverses after half a period; hence translation by $\frac{1}{2}P$ in time is equivalent to either of the symmetries that were broken at the Hopf bifurcation. (Purely temporal symmetries are discussed in more detail in the Appendix; note that nonlinear solutions do not have any reflection symmetry in time (McKenzie 1988).) So we obtain three further symmetry operations:

$$t_x = m_x t_e: \quad (x,z,t) \to (\lambda - x, z, t+\tfrac{1}{2}P), \quad (\Psi, \Theta, \Sigma) \to (-\Psi, \Theta, \Sigma), \tag{18}$$

$$t_z = m_z t_e: \quad (x,z,t) \to (x, 1-z, t+\tfrac{1}{2}P), \quad (\Psi, \Theta, \Sigma) \to (-\Psi, -\theta, -\Sigma), \tag{19}$$

$$t_i = i t_e: \quad (x,z,t) \to (\lambda - x, 1-z, t+\tfrac{1}{2}P), \quad (\Psi, \Theta, \Sigma) \to (\Psi, -\Theta, -\Sigma). \tag{20}$$

The symmetry operations $\{E, m_x, m_z, i, t_x, t_z, t_i, t_e\}$ form the eighth-order orthorhombic group $D_{2h} = D_2 \otimes Z_2$ (corresponding to the symmetry of a cuboid) whose multiplication table is exhibited in table 2. This abelian symmetry group describes the interactions with which we are concerned.

The group has seven fourth-order invariant subgroups, each of which is isomorphic to D_2. They describe the symmetries of pure steady and periodic solutions. Thus steady single-roll (*is*) solutions have the symmetries $\{E, i, t_i, t_e\}$, while steady two-roll (*xs*) and stacked-roll (*zs*) solutions have symmetries $\{E, m_x, t_x, t_e\}$ and $\{E, m_z, t_z, t_e\}$, respectively. Periodic single-roll (*io*) solutions have the symmetries $\{E, i, t_x, t_z\}$, while periodic two-roll (*xo*) and stacked-roll (*zo*) solutions have symmetries $\{E, m_x, t_z, t_i\}$ and $\{E, m_z, t_i, t_x\}$, respectively. The group $\{E, m_x, m_z, i\}$ describes periodic four-roll solutions, which do not concern us.

The D_2 symmetry of one of these pure solutions may be broken at a secondary bifurcation leading to solutions with Z_2 symmetry only. Thus the symmetry of a pure steady single-roll (*is*) solution could be broken at a pitchfork bifurcation to give steady mixed-mode solutions with symmetry t_e or at a Hopf bifurcation to give either pure periodic solutions with symmetry i or mixed-mode periodic solutions with symmetry t_i. Similarly, the symmetry of a pure periodic single-roll (*io*) solution can be broken at a pitchfork bifurcation to give either a pure, temporally asymmetric, periodic solution with the symmetry i, or mixed-mode periodic solutions with the symmetry t_x or the symmetry t_z. The Z_2 symmetries may themselves subsequently be broken at a tertiary bifurcation.

Mixed-mode solutions can serve to transfer stability from one branch of pure solutions to another. In addition to classifying different solutions we can predict the symmetry properties of mixed-mode solutions on a branch connecting two branches of pure periodic solutions. For instance, mixed-mode periodic solutions on a branch linking the *io* and *xo* branches must have the symmetry t_z which is common to both families of pure solutions. Similarly, mixed modes linking *io* and *zo* solutions must have the symmetry t_x. Another possibility is that the branch of oscillatory solutions originates in a secondary Hopf bifurcation from a branch of steady solutions. In magnetoconvection pure two-roll solutions with the Z_2 symmetry group $\{E, m_x\}$ bifurcate from the branch of *xs* solutions. These oscillations are vacillatory but they eventually gain the full symmetry of *xo* solutions in a global gluing (or biclinic) bifurcation (Nagata *et al.* 1990). In the same way, mixed-mode oscillations with the symmetry t_z bifurcate from the *xo* branch and lose their symmetry in a biclinic bifurcation to give periodic solutions with the trivial symmetry E only, on a branch which meets the branch of asymmetric steady solutions in a Hopf bifurcation (cf. figure 13 of Nagata *et al.*).

Periodic solutions can be represented by expanding the coefficients in (10)–(12) as Fourier series with the form

$$a_{mn}(t) = \sum_{-\infty}^{\infty} a_{lmn} \exp(2\pi i l t/P) \quad \text{etc.} \tag{21}$$

Then it follows from (17) that solutions with the symmetry t_e must have $a_{lmn} = b_{lmn} = d_{lmn} = 0$ for l odd; in fact we know that steady solutions have non-zero coefficients only for $l = 0$. Similarly, from (18), the symmetry t_x implies that $a_{lmn} = b_{lmn} = d_{lmn} = 0$ for $l+m$ odd, while, from (19) and (20), t_z and t_i imply that the coefficients in (21) are zero for $l+n$ odd and $l+m+n$ odd, respectively. It follows that *xo* solutions have non-zero coefficients for m even and $l+n$ even, *zo* solutions for n even and $l+m$ even, and *io* solutions for $l+m$ even and $l+n$ even. These conditions can be used to identify the symmetries of periodic solutions in numerical experiments (cf. Jennings & Weiss 1991).

3. Solutions with point symmetry

We investigate nonlinear behaviour by solving the partial differential equations numerically. The code differs only slightly from that employed by Knobloch *et al.* (1986*b*, hereinafter referred to as I). The parabolic equations (2)–(4) are solved using a centred finite-difference scheme with second-order accuracy in space and time on a mesh with equal intervals in x and z; the code uses a leapfrog scheme with the Jacobians treated explicitly and the diffusive terms represented by a Dufort–Frankel scheme (Moore, Peckover & Weiss 1974). The Poisson equation (5) is solved using fast Fourier transforms and tridiagonal inversion. This scheme provides an effective means of exploring behaviour in different regions of parameter space, where many different runs are needed. As the mesh is refined, however, our second-order scheme converges painfully slowly in comparison with higher-order difference schemes or spectral methods. The code is structured so as to enhance efficiency on vector processors like the Cray, with each variable defined on four interlocking spatial meshes. The mesh interval $\Delta z = N_z^{-1}$ and $N_x = \lambda N_z$. The timestep $\Delta t = N_t^{-1}$ is limited by accuracy requirements for the diffusive term and we set $\Delta t \approx 0.4 \Delta z^2$ (Moore *et al.* 1990*b*). For most of the computations presented here we had $N_z = 32$, $N_x = 48$, $N_t = 2500$. This mesh has sufficient resolution to give qualitatively accurate results. The value of R_T at a typical codimension-one bifurcation is displaced by ΔR_T from its asymptotic position in the limit as $\Delta z \rightarrow 0$ and we find that $\Delta R_T \leqslant 20$ (Moore, Weiss & Wilkins 1990*a*, *b*). Certain period-doubling bifurcations are more sensitive to discretization. Where necessary we have therefore refined the mesh and obtained results with $N_z = 64$ and 128.

	R_T	10700	10750	10800	11000	11500	12000
(a)	N_T	3.02	3.10	3.16	3.34	3.62	3.84
	V	22.41	23.37	24.10	26.26	30.10	33.17
(b)	N_T	—	3.00	3.09	3.30	3.61	3.83
	V	—	22.14	23.24	25.75	29.77	32.91

TABLE 3. Steady solutions with point symmetry for $R_S = 10^4$, $\lambda = 1.5$. (a) Second-order finite-difference scheme. (b) Accurate mixed scheme

To provide global measures of nonlinear behaviour we use the r.m.s. velocity V given by

$$V^2 = \frac{1}{2\lambda}\int_0^1\int_0^\lambda |\nabla\Psi|^2\,dx\,dz = \frac{1}{2\lambda}\int_0^1\int_0^\lambda \Psi\omega\,dx\,dz \tag{22}$$

and the solutal Nusselt number N_S or the thermal Nusselt number N_T, where

$$N_S = 1-\lambda^{-1}\int_0^\lambda \partial_z\Sigma\,dx, \quad N_T = 1-\lambda^{-1}\int_0^\lambda \partial_z\Theta\,dx, \tag{23}$$

both evaluated at either the lower or the upper boundary ($z = 0, 1$). Values of N_S are typically higher than N_T but N_T displays more interesting time-dependent structure. Deviations from point symmetry can be detected by monitoring the mean temperature $\bar{\Theta}$ or the mean solute concentration $\bar{\Sigma}$ at the middle of the layer ($z = \frac{1}{2}$), since it follows from (1) that these quantities vanish for symmetrical solutions.

3.1. *Steady solutions*

Modified perturbation theory can be used to find weakly nonlinear solutions in the neighbourhoods of bifurcations from the trivial solution (Huppert & Moore 1976; Da Costa, Knobloch & Weiss 1981). The pitchfork bifurcations are, strictly speaking, supercritical though R_T decreases along the (non-stable) steady branches in all four cases. Since the trivial solution is globally attracting for $R_T < R_0$ (Joseph 1976) each steady branch must turn round in a saddle-node bifurcation at $R_T = R_T^{(\mathrm{min})}$ ($R_0 < R_T^{(\mathrm{min})} < R_T^{(e)}$). We shall refer to steady convection with $R_T^{(\mathrm{min})} \leqslant R_T < R_T^{(e)}$ as subcritical.

All steady solutions that we have found are of type *is* and possess the point symmetry *i*. They are therefore identical with solutions found at lower resolution with that symmetry explicitly imposed in I, and similar to those described by Huppert & Moore (1976) for $\lambda = \sqrt{2}$. We have tested the stability of these solutions by adding asymmetric perturbations to the temperature field. In all cases the value of $\bar{\Theta}$ dropped rapidly to zero, confirming that these solutions are stable to such perturbations. These stable steady solutions exist for $R_T > R_T^{(\mathrm{min})}$; at $R_T = R_T^{(\mathrm{min})}$ there is a saddle-node bifurcation, with a branch of unstable steady solutions covering the range $R_T^{(\mathrm{min})} < R_T < R_T^{(e)}$. For $N_z = 32$ we find that $10650 < R_T^{(\mathrm{min})} < 10700$. This is slightly higher than the value ($R_T^{(\mathrm{min})} \approx 10450$) obtained by Huppert & Moore (1976) with $\lambda = \sqrt{2}$. In table 3 we list values of N_T and V along the steady branch, obtained using finite differences with $N_z = 32$. These are compared with accurate values calculated using a Fourier expansion with 16 modes in the x-direction and a fourth-order implicit Runge–Kutta finite-difference scheme (Cash & Moore 1980) with $N_z = 32$ in the vertical direction. With this more accurate method

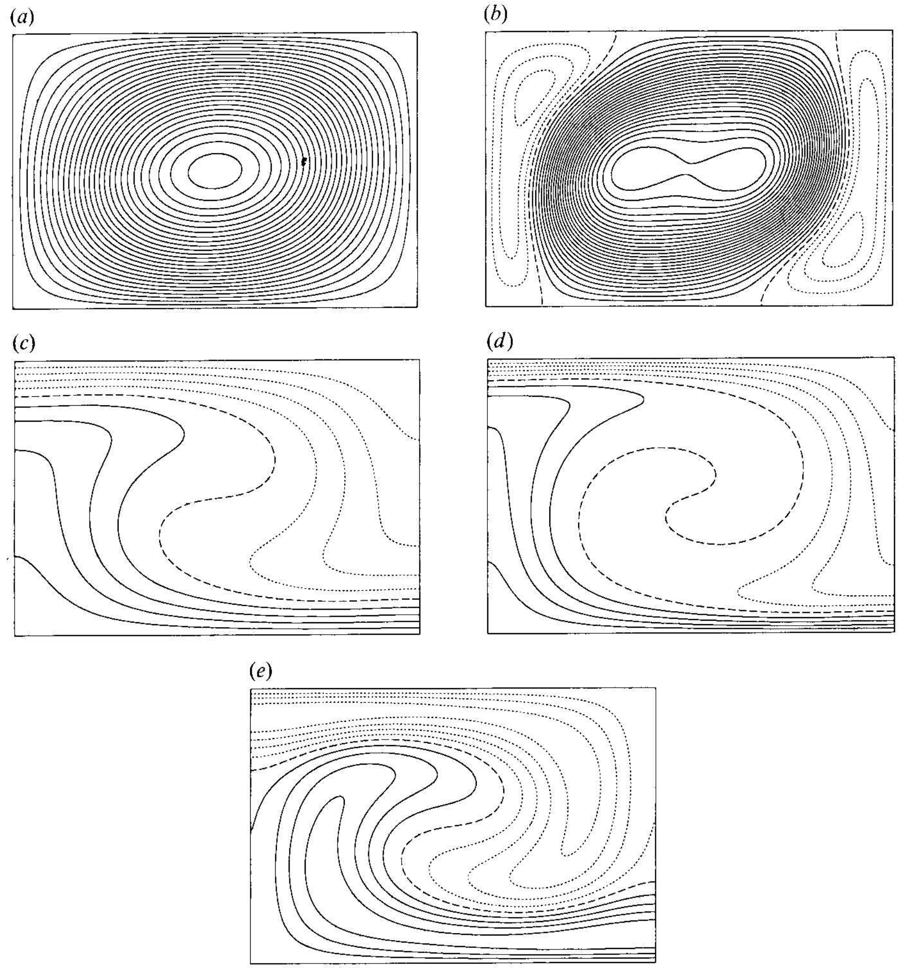

FIGURE 1. Steady convection: the stable symmetric (*is*) solution at $R_T = 10800$. Contours of (*a*) Ψ (streamlines), (*b*) the vorticity ω, (*c*) T (isotherms), (*d*) the solute concentration S and (*e*) the density ρ. Full (dotted) lines denote positive (negative) values and the zero contour is broken.

(which is only available for steady solutions) we find that $R_T^{(\min)} \approx 10730$. So our second-order finite-difference scheme, with $N_z = 32$, displaces the value of R_T at the saddle-node bifurcation by about 0.6%. (The error here is three times larger than the typical value quoted above.) Table 3 shows that the second-order scheme overestimates the global quantities N_T and V. The errors are greatest (3.3% and 5.6% respectively) near the saddle-node bifurcation but drop to 0.3% and 0.8% at $R_T = 12000$.

Figures 1(*a*), 1(*b*), 1(*c*) and 1(*d*) illustrate the spatial variation of the fields Ψ, ω, T and S for the steady solutions at $R_T = 10800$. In addition we show in figure 1(*e*) the normalized density field

$$\rho = R_S S - R_T T. \tag{24}$$

Solid (broken) contours indicate positive (negative) values and the zero contour is dotted. At the bottom boundary ($z = 0$) $T = S = \frac{1}{2}$ and $\rho = -\frac{1}{2}(R_T - R_S)$ while at the top ($z = 1$) $T = S = -\frac{1}{2}$ and $\rho = \frac{1}{2}(R_T - R_S)$. In the regime that we are interested in the density stratification is weakly unstable. Point symmetry of the solution is apparent from the figure. The region is occupied by a single eddy rotating clockwise. (An equivalent solution with the opposite sense of rotation is generated by m_x or m_z.) This produces broad thermal plumes in which are embedded narrow solutal plumes and the central region has an almost uniform solute concentration ($S \approx 0$). The density has more structure, with extrema at the edges of the solute plumes, where light (heavy) fluid rises (sinks) to drive the motion. More precisely, we see from (2) that vorticity generation is proportional to $\partial\rho/\partial x$. Hence positive vorticity is generated in the central region (where $\partial\rho/\partial x > 0$) while negative counter-vorticity is generated at the edges, with the results shown in figure 1(*b*). Consequently the eddy is weaker at the edges of the cell and the vertical speed is greatest near the centres of the density plumes. This pattern is distinctly nonlinear and quite different from the linear eigenfunctions which describe weakly nonlinear solutions near the stationary bifurcation.

It seems clear that there must be unstable steady solutions in which point symmetry is broken, as we shall explain in §7. In such solutions the rising and sinking plumes would no longer be equivalent and the centre of the eddy would be displaced towards one side of the region, as in magnetoconvection (Weiss 1981). We have not attempted to compute these solutions.

3.2. *Oscillations and temporal chaos*

From the supercritical Hopf bifurcation at $R_T^{(o)}$ there emerges a branch of periodic oscillations with period P. Oscillatory solutions on this branch are of type *io* and possess the point symmetry i. Moreover, since clockwise and anticlockwise motions are equivalent, advancing time by half a period is equivalent to the symmetries m_z or m_x. Hence they also possess the temporal symmetries t_z and t_x. It follows from (19) that the kinetic energy V^2 has a period $\frac{1}{2}P$ and that

$$N_T(z=0,t) = N_T(z=1,t+\tfrac{1}{2}P), \quad N_S(z=0,t) = N_S(z=1,t+\tfrac{1}{2}P). \tag{25}$$

It also follows from (15) that

$$N_T(z=0,t) = N_T(z=1,t), \quad N_S(z=0,t) = N_S(z=1,t). \tag{26}$$

From (25) and (26) the Nusselt numbers at the upper and lower boundaries are therefore equal and vary with period $\frac{1}{2}P$. In what follows we measure N_S and N_T at $z=1$ unless stated otherwise.

The branch of symmetric oscillations terminates in a heteroclinic bifurcation involving saddle-foci on the unstable segment of the steady branch. Before then it has become unstable to perturbations in which first the temporal symmetries t_z and t_x and then the spatial symmetry i are broken. We find that for $R_T^{(o)} < R_T \leqslant 10675$ all stable solutions retain the point symmetry (15). In particular, numerical solutions obtained by solving (2)–(7) over the full domain $\{0 \leqslant x \leqslant \lambda; 0 < z < 1\}$ are identical with those obtained for the same N_z and N_t by integrating over the region $\{0 \leqslant x < \frac{1}{2}\lambda; 0 < z < 1\}$ and applying the symmetry (15) explicitly, as in I. So we shall first consider bifurcations in which temporal symmetries are broken and then discuss the loss of spatial symmetry in the next section. Note that period doubling is preceded by loss of temporal symmetry; this process can also be related to an appropriate symmetry group (McKenzie 1988), as indicated in the Appendix.

The behaviour of solutions with point symmetry explicitly imposed was investigated systematically in I using a mesh with $N_z = 16$; some runs were checked with $N_z = 32$ in order to confirm that the bifurcation structure was robust. We have not attempted to repeat all these calculations, though some details have been studied at higher resolution. Solutions on the branch emerging from the initial Hopf bifurcation lose stability at $R_T \approx 9150$, where the temporal symmetry (16) is broken in a pitchfork bifurcation. The period of the quadratic quantities V^2, N_T and N_S is doubled as a result. Successive period-doubling bifurcations then lead to chaos, followed by an inverse cascade which ends with a temporally asymmetric (P1) solution at $R_T = 10400$ and a symmetric (S1) solution at $R_T = 10500$. This first bubble of chaos is sensitive to discretization but a careful study has confirmed that a narrow interval of chaos around $R_T = 10200$ persists as $\Delta z \rightarrow 0$ (Moore *et al.* 1990*b*).

This segment of the oscillatory branch terminates at $R_T \approx 10500$ and trajectories are attracted to a second segment with different periodic solutions. Stable S1 solutions appear in a saddle-node bifurcation around $R_T = 10300$, followed by symmetry-breaking and a further cascade of period-doubling bifurcations which leads to chaotic behaviour interspersed with narrow periodic windows. The existence of chaos for $\lambda = 1.4$ has been conclusively established by showing that the positions of windows with symmetrical period-five (S5) and period-three (S3) solutions converge to different values of R_T as $N_z \rightarrow \infty$ (Moore *et al.* 1990*b*). Since periodic solutions appear in the order familiar from quadratic maps these results show that all periods must exist together with related intervals of chaos (cf. Proctor & Weiss 1990). Note, however, that the nature of the solution at a fixed value of R_T will change with the mesh spacing as different windows drift by. Thus we expect to find different behaviour within the chaotic regime for $\lambda = 1.5$ with $N_z = 16$ and $N_z = 32$. With $N_z = 32$ we have obtained a period-two (P2) solution for $R_T = 10500$, chaotic solutions for $R_T = 10600$, 10650, and an S3 periodic solution for $R_T = 10700$; all these solutions have point symmetry and are stable to asymmetric perturbations.

With point symmetry explicitly imposed we find chaotic behaviour for $R_T =$ 10800, 10900, 11000. At $R_T = 11100$ there is a P2 solution, forming part of a period-doubling cascade whose accumulation point shifts from $R_T \approx 11055$ to $R_T \approx 11123$ as the number of mesh intervals increases from $N_z = 16$ to $N_z = 128$ (Moore *et al.* 1990*a*). Finally, for $R_T = 11200$ trajectories are attracted to the steady branch. This pattern of behaviour and the form of the solutions allow us to infer the existence of a heteroclinic connection between two saddle-foci at $R_T \approx 11200$, as proposed in I.

4. Asymmetric oscillations

4.1. *Loss of spatial symmetry*

When the point-symmetric S3 solution at $R_T = 10700$ is perturbed the spatial asymmetry rapidly disappears ($|\bar{\Theta}| < 10^{-5}$) but for $R_T = 10750$ there is an aperiodic solution with $|\bar{\Theta}| \approx 0.003$ and this slight spatial asymmetry does not decay. For $R_T = 10800$, 10850, 10900 there is asymmetric chaos with $|\bar{\Theta}| \approx 0.02$. Figure 2(*a*) shows a trajectory for $R_T = 10800$ projected onto the (V, N_T)-plane. The chaotic attractor differs slightly (but perceptibly) from that for the same value of R_T with point symmetry explicitly imposed. In figure 3 we illustrate the typical spatial structure of the solutions after point symmetry is broken. The streamlines and the contours of S show a small but noticeable asymmetry, most apparent in the positions of eddy centres in figure 3(*a*) or the dotted zero-contours of S in figure 3(*b*).

As R_T is further increased there is a change in the nature of the spatially asymmetric solutions. For $R_T = 10950$, 11000, 11100 small asymmetric perturbations develop, after transient chaos, into periodic oscillations. This transition

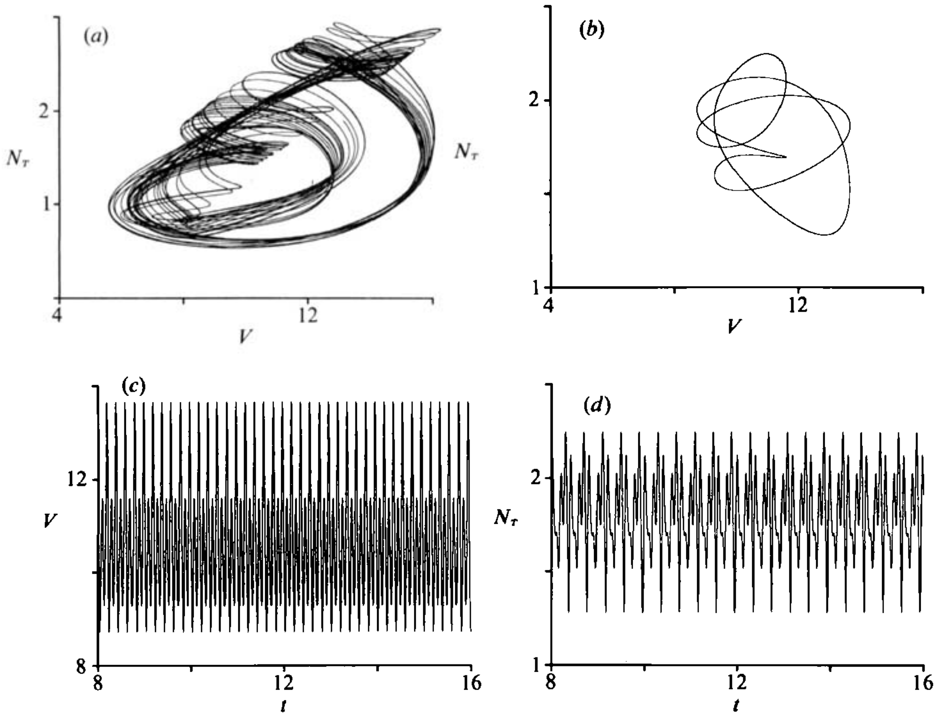

FIGURE 2. Spatially asymmetric solutions at $R_T = 10800$. Phase portraits projected onto the (V, N_T)-plane for (a) a slightly asymmetric chaotic trajectory and (b) an asymmetric S1 orbit with symmetry t_z. Time series for the periodic S1 solution, showing (c) V and (d) N_T as functions of time t.

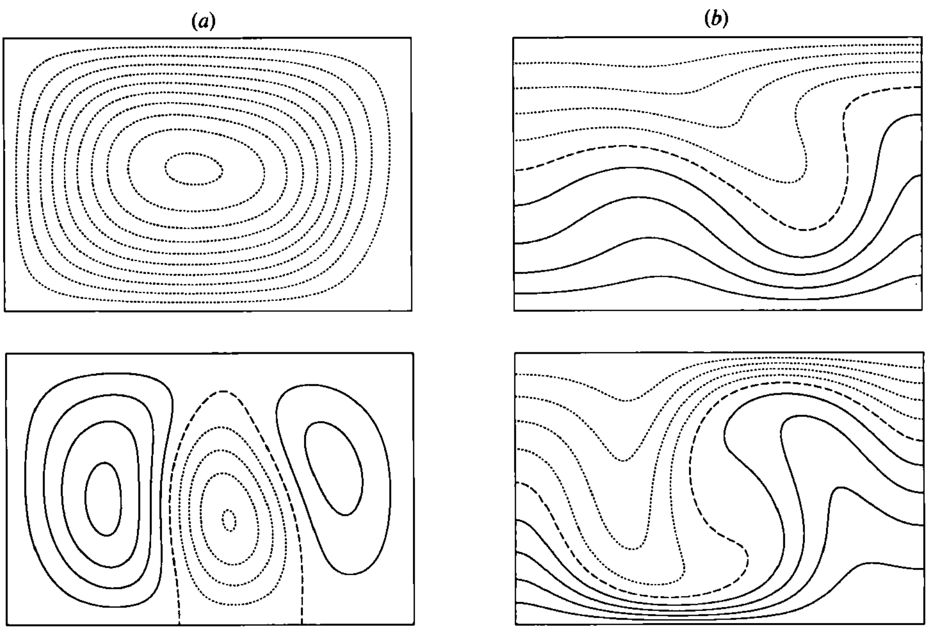

FIGURE 3. Loss of spatial symmetry in the aperiodic solutions at $R_T = 10800$. Contours of (a) Ψ and (b) S at two different times.

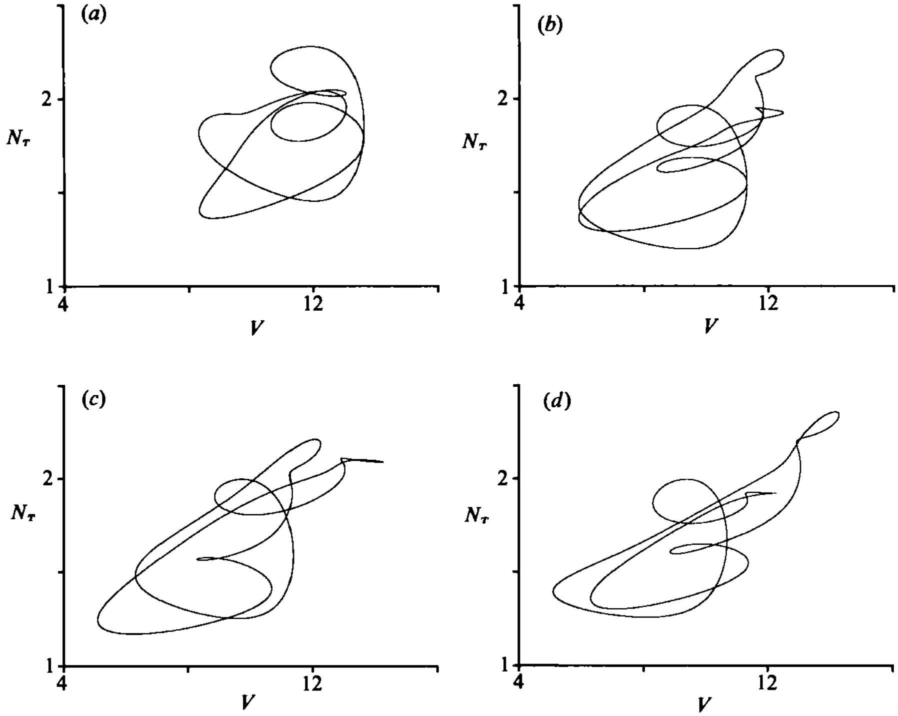

FIGURE 4. Phase portraits for spatially asymmetric periodic solutions. Solutions with temporal symmetry t_z at $R_T = 11500$ on (*a*) the first segment and (*b*) the second segment of the asymmetric S1 branch. Loss of temporal symmetry is shown by the equivalent orbits for P1 solutions at $R_T = 11600$ with (*c*) N_T at $z = 1$ and (*d*) N_T at $z = 0$.

has been followed by Moore *et al.* (1990*a*) for $R_T = 11100$ and apparently similar behaviour was reported by Shi & Orszag (1987). These new solutions lie on a branch that extends over the range $10690 \leqslant R_T \leqslant 11560$. Figure 2(*b*) shows a characteristic orbit, for $R_T = 10800$, which differs significantly from any found for solutions with point symmetry. We notice first that the trajectory apparently describes a double cycle in which the maxima and minima of V are exactly repeated for different values of N_S. The two time series in figures 2(*c*) and 2(*d*) confirm that V^2 repeats each cycle (corresponding to clockwise or anticlockwise motion) exactly and has period $\frac{1}{2}P$ while N_T has period P. This is precisely what should be expected from an S1 solution that possesses the temporal symmetry (19) but lacks the spatial symmetry (15). It can moreover be confirmed that the Nusselt numbers at the top and bottom of the layer differ in phase by half a period, as predicted by (25).

These symmetry properties permit us to distinguish between two different types of spatially asymmetric oscillations, corresponding to different mixed-mode solutions. The solutions we have found have the temporal symmetry t_z. Hence they correspond to mixed-mode solutions on branches bifurcating from the branches of pure single-roll (*io*) or two-roll (*xo*) solutions, with symmetries i and m_x respectively. If advancing time by half a period were instead equivalent to the symmetry operation m_x we would immediately obtain the temporal symmetry t_x. It would then follow that

$$N_T(z=0,t) = N_T(z=0,t+\tfrac{1}{2}P), \quad N_T(z=1,t) = N_T(z=1,t+\tfrac{1}{2}P) \tag{27}$$

etc. but there would be no equivalence between Nusselt numbers measured at the top and bottom of the layer. Such mixed-mode solutions would involve pure single-roll solutions and solutions with two stacked rolls, with symmetries i and m_z respectively.

4.2. *Mixed-mode periodic solutions*

If the trivial solution is perturbed for $10950 \leqslant R_T \leqslant 11150$ the unstable modes possess point symmetry and develop into periodic or aperiodic spatially symmetric oscillations. These are in turn unstable to spatially asymmetric perturbations and gradually evolve into periodic oscillations that lack spatial symmetry but possess the temporal symmetry t_z. This process is particularly clear for $R_T = 11100$, where the spatially symmetric oscillation is also periodic (Moore *et al.* 1990*a*). Using the stable asymmetric S1 solution at $R_T = 11000$ to provide initial conditions we have followed the branch of S1 solutions down to $R_T = 10690$. For $R_T = 10675$ the only stable solution is a spatially symmetric but temporally asymmetric P3 oscillation. (The form of this solution indicates that is belongs to the inverse cascade associated with the stable S3 solution at $R_T = 10700$). When R_T is increased the S1 solutions continue up to $R_T = 11560$ but trajectories for $R_T = 11580$ are eventually attracted to a different solution. The S1 solutions evolve gradually along the branch from $R_T = 10690$ to $R_T = 11560$ and their spatial structure remains essentially similar. The orbit at $R_T = 10690$ differs only slightly from that for $R_T = 10800$ in figure 2(*b*) and the changing lobe structure can be followed from the beginning to the end of this segment of the S1 branch. Figure 4(*a*) shows the phase portrait at $R_T = 11500$.

The spatial structure of these periodic solutions is depicted in figures 5 and 6 for $R_T = 10800$. Figures 5(*a*), 5(*b*) and 5(*c*) show contours of Ψ, T and S at six equally spaced intervals spanning half a period. The first and last frames are related by the temporal symmetry (16) which can be used to reconstruct contours for the next half-period. The streamlines show a single major eddy which is reversed as an eddy with the opposite sense of motion migrates across the domain from right to left. (There is of course an equivalent solution, related to this by the symmetry operation i, in which the eddies migrate from left to right.) The temperature and solute concentration are fairly well-behaved, with rising and falling plumes in the left half of the region and relatively little structure on the right. This is the characteristic form of mixed-mode solutions involving a combination of single-roll and two-roll modes which combine constructively in one half of the cell and cancel in the other so as to produce a left–right asymmetry.

Figure 6 shows that the dynamics is really more complicated. The density contours in figure 6(*a*) demonstrate that ρ has far more spatial structure than either T or S. The isolated maximum near the upper boundary develops into a massive plume that plunges downwards and disintegrates, to be succeeded by an equivalent buoyant plume that rises from the lower boundary. Contours of ω in figure 6(*b*) show that vorticity generation is dominated by these prominent rising and sinking plumes but the contours are distorted as vorticity is advected by the flow.

These details illustrate how differences between smoothly varying thermal and solutal fields produce strong density gradients with a complicated spatial structure. Thus it is not surprising that the system exhibits a great variety of dynamical behaviour. Near the Hopf bifurcation at $R_T^{(o)}$ the symmetric oscillations have a simple spatial structure with a single eddy that grows, decays and then reverses without change of form, as kinetic energy is transformed to potential energy and back again. In the fully nonlinear regime counter-vorticity is generated near both edges of the region, as in the steady solution of figure 1, and then spreads inwards to reverse the

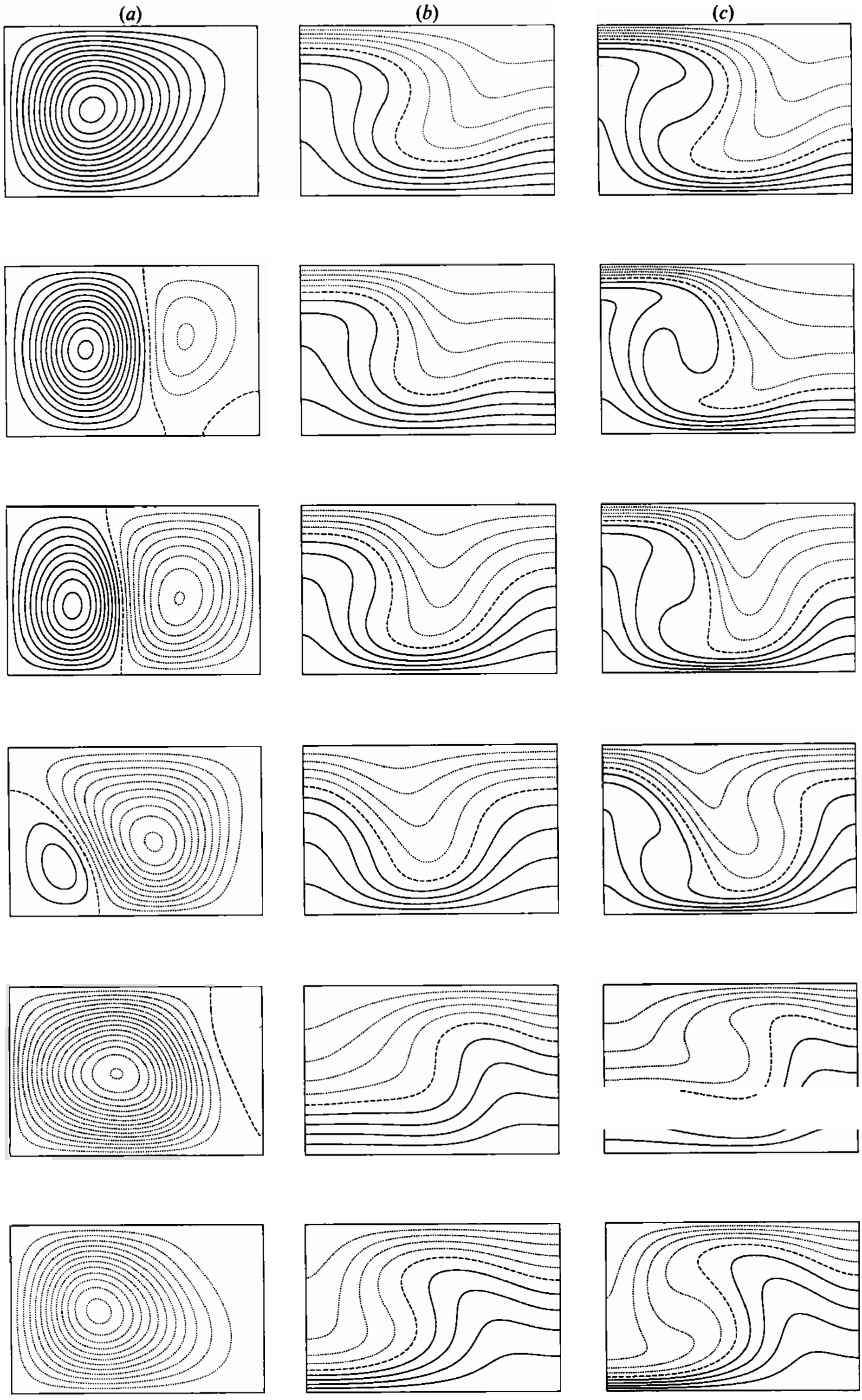

FIGURE 5. Spatial structure for the S1 solution at $R_T = 10800$. Contours of (*a*) Ψ, (*b*) T and (*c*) S at equally spaced intervals of $0.1P$ in time. Loss of point symmetry is apparent. Note that the first and last sets are related by the symmetry t_z.

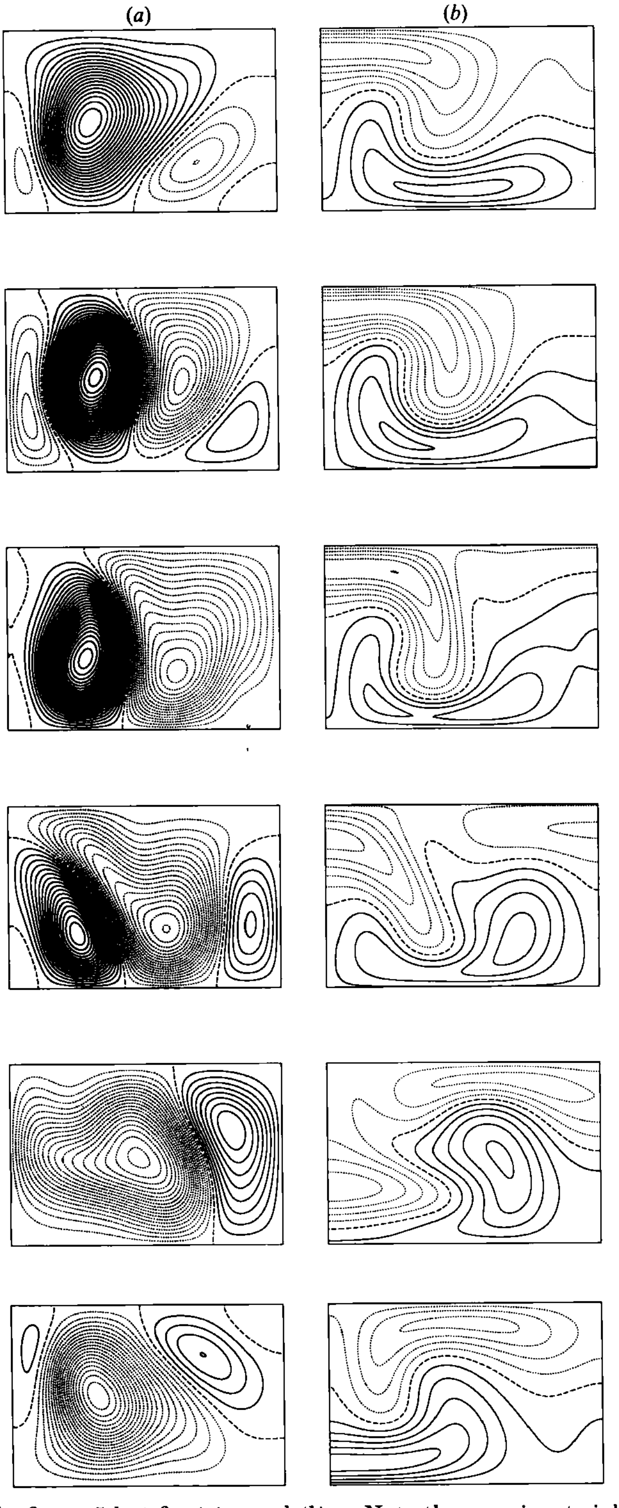

FIGURE 6. As figure 5 but for (a) ρ and (b) ω. Note the prominent sinking plume and its effect on the vorticity.

motion (cf. Moore *et al.* 1990*a*). Symmetry breaking implies that the system favours a configuration in which counter-vorticity affects only one side of the eddy. Nevertheless, peak values of N_T and of V are significantly greater for the unstable point-symmetric solutions than for the stable S1 oscillations, as can be seen (approximately) by comparing figure 2(*a*) with figure 2(*b*). Analogous behaviour is found in magnetoconvection.

The S1 solutions appear at $R_T = 10690$ with significant asymmetry and a characteristic form. Hence there has to be a saddle-node bifurcation at $R_T \approx 10680$. We presume that the unstable segment of the asymmetric S1 branch bifurcates subcritically from the original symmetric S1 branch for $R_T \geqslant 10750$, perhaps in some narrow interval where point-symmetric S1 solutions are stable to spatially symmetric perturbations. Any branch that subsequently bifurcates from the symmetric S1 branch will then be unstable to asymmetric perturbations, so we expect cascades of period-doubled solutions and the chaotic solutions beyond their accumulation points to be unstable. On the other hand, periodic solutions that appear in saddle-node bifurcations need not share the stability properties of the S1 branch, so symmetric solutions may persist in isolated windows. Conversely, asymmetric solutions may exist where the original S1 solution is still stable to asymmetric perturbations. This may explain the weakly asymmetric but apparently stable chaotic behaviour found around $R_T = 10800$ and illustrated in figure 3. Such solutions are likely to be sensitive to discretization but we have not investigated them in any detail.

5. Loss of temporal symmetries

For $R_T = 11500$ there are two distinct spatially asymmetric S1 solutions with very different limit cycles. The first, shown in figure 4(*a*), corresponds to the S1 solutions that have already been described, on a segment of the solution branch which ends at $R_T \approx 11570$. The second, shown in figure 4(*b*), has an extra kink in each cycle but still retains the temporal symmetry t_z. The spatial structure of these solutions resembles that in figures 5 and 6 for $R_T = 10800$ though the asymmetry is more marked. The solutions are on a second segment which can be followed down to $R_T = 11350$; for $R_T = 11330$ trajectories are attracted to an orbit like that in figure 4(*a*). The two stable segments of the S1 solution branch are apparently connected by an unstable segment which meets them in saddle-node bifurcations at $R_T \approx 11340$ and $R_T \approx 11570$. The resulting structure of the S1 branch is shown schematically in figure 7, where the period of the solutions is plotted as a function of R_T.

S1 solutions on the upper segment in figure 7 remain stable until $R_T \approx 11535$, when the temporal symmetry t_z is broken in a pitchfork bifurcation. The resulting asymmetry is apparent in the spatial form of the solutions which only retain the trivial symmetry E. Figure 8 shows contours of Ψ and S at two pairs of times separated by an interval of $\frac{1}{2}P$ for $R_T = 11600$. The symmetry of the velocity and solute concentration in figure 5 has clearly been broken. This bifurcation is also indicated in figure 7.

The bifurcation gives rise to two branches of P1 solutions, related by the broken symmetry t_z. Figure 4(*c*) shows a P1 orbit for $R_T = 11600$, projected onto the (V, N_T)-phase plane. The kinetic energy now has a period P and the extrema of V are no longer equal on successive cycles, as they were for $R_T = 11500$ in figure 4(*b*). It is apparent from figure 8 that (25) no longer applies and there is no equivalence between Nusselt numbers at the top and bottom of the layer. (The conservation laws (3) and (4) still ensure that the time-averaged Nusselt numbers are independent of

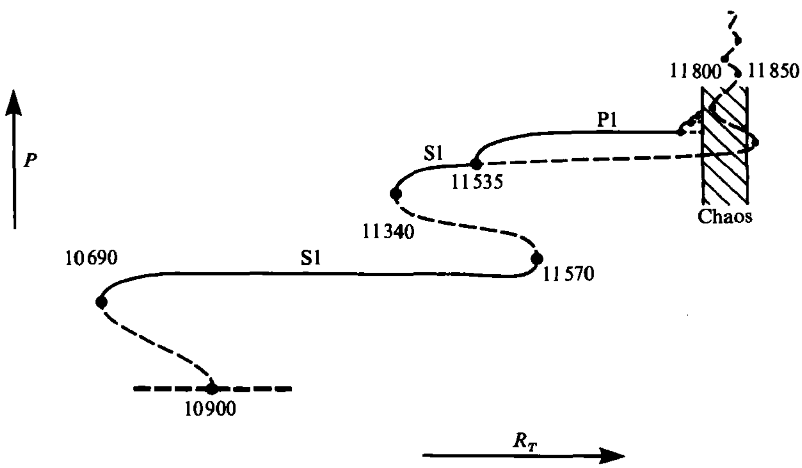

FIGURE 7. Schematic bifurcation structure for the spatially asymmetric oscillatory solutions, showing the period P as a function of R_T. Solid (broken) lines denote stable (unstable) solutions and the branch of symmetric S1 solutions is indicated by a heavy line.

z.) Hence the phase portrait obtained using $N_T(z=0,t)$, shown in figure 4(*d*), differs from that for $N_T(z=1,t)$ in figure 4(*c*). Now the two P1 solutions are related by the symmetry m_z, since phase differences can be ignored, so there is also an alternative solution in which $N_T(z=1,t)$ yields the orbit in figure 4(*d*) while $N_T(z=0,t)$ gives that in figure 4(*c*). Which of these two solutions is preferred depends on the initial conditions, and trajectories may flip from one to the other before being attracted to a limit cycle. If one is attempting to follow the P1 solution branch by computing trajectories in the plane with coordinates V and $N_T(z=1)$ then it is not apparent that the two periodic orbits in figures 4(*c*) and 4(*d*) are equivalent until one recognizes that the extremal values of V are identical.

The P1 solution branch undergoes further bifurcations which are sensitive to discretization. For $N_z = 32$ we find a bubble with P2 solutions at $R_T = 11540$, 11590 and a narrow band of chaos centred on $R_T = 11570$. When the mesh spacing is halved, so that $N_z = 64$, the P1 branch remains stable throughout this range. As R_T is further increased stable P1 solutions persist without change of form up to $R_T = 11720$. For $N_z = 32$ there follows a cascade of period-doubling bifurcations, with a P2 solution at $R_T = 11730$, P4 at $R_T = 11733$ and chaotic behaviour over the interval $11736 \leqslant R_T \leqslant 11830$. For $R_T \geqslant 11850$ trajectories are attracted to the spatially symmetric steady solution. For $N_z = 64$ the bifurcations are displaced to somewhat higher values of R_T, with a P2 solution at $R_T = 11770$, P4 at $R_T = 11780$ and aperiodic behaviour at $R_T = 11785$. Finally, with $N_z = 128$ (so $N_x = 192$ and $N_t = 4\times 10^4$) we recover P2 solutions for $11775 \leqslant R_T \leqslant 11795$ but obtain an apparently chaotic solution at $R_T = 11800$. So it is likely but not certain that the bifurcation values have converged.

For our choice of parameters it seems that asymmetric chaos is marginal. By analogy with the constrained case we expect that stable aperiodic behaviour exists nearby in parameter space over a wider range in R_T. Moreover, the wiggles along the S1 branch, where the trajectory in figure 4(*b*) winds once more round the non-stable fixed points than that in figure 4(*a*), are consistent with the approach to a heteroclinic connection between two saddle-foci, with eigenvalues that satisfy Shil'nikov's criterion (Wiggins 1988). We assume, therefore, that the branch ends as

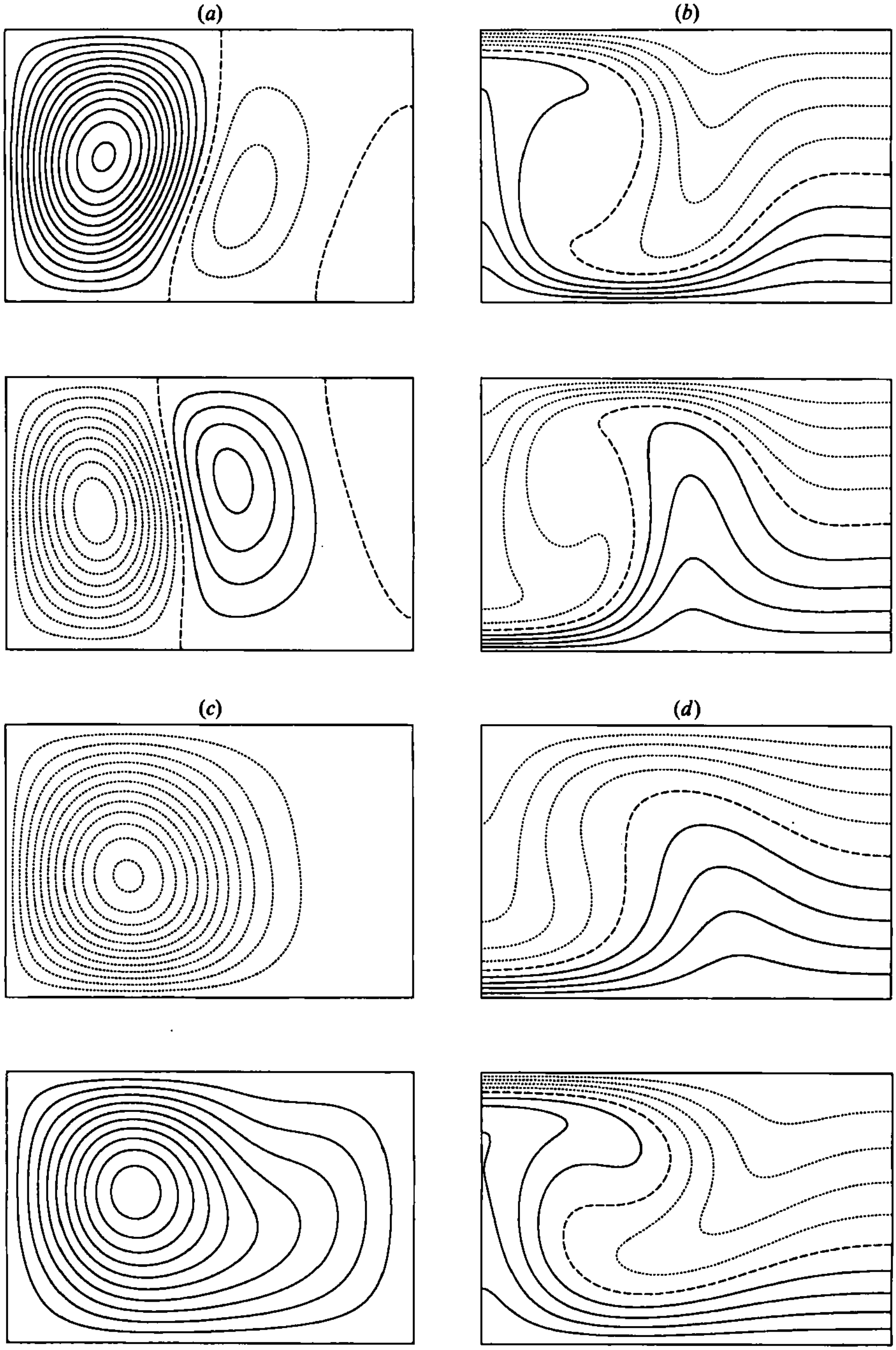

FIGURE 8. Spatial and temporal asymmetry for a P1 solution at $R_T = 11600$. Contours of (*a*) Ψ and (*b*) S for a pair at two instants separated by an interval $\frac{1}{2}P$. (*c*), (*d*) The same but for a second pair displaced in phase by $0.2P$ relative to the first pair. The temporal symmetry t_z has been broken.

shown in figure 7 and that chaos is produced by the Shil'nikov mechanism once again.

6. Bifurcation structure

We have shown how as systematic sequence of numerical experiments can be used to determine the symmetries of oscillatory solutions in this problem and to locate the bifurcations where these symmetries are broken. The properties of the spatially asymmetric oscillations are consistent with our assertion that they are mixed-mode solutions on a branch that bifurcates from the pure single-roll branch. This could only be verified by following the various unstable branches of time-dependent single-roll, two-roll and mixed-mode solutions – a formidable task for the partial differential equations. What is feasible is to follow the branches of steady solutions. It turns out that they engage in resonant interactions with three-roll solutions too, generating convoluted bifurcation structures which will be described elsewhere.

In the analogous case of magnetoconvection, where point symmetry is likewise broken, numerical experiments yield a continuous sequence of transitions from oscillatory two-roll to oscillatory mixed-mode to steady mixed mode and finally to steady single-roll solutions (Weiss 1981). Moreover, the full bifurcation structure has been established for a seventeenth-order truncated model system (Nagata *et al.* 1990). The agreement between behaviour in this (relatively) low-order system and in the partial differential equations confirms that symmetry breaking does indeed correspond to the appearance of mixed-mode solutions. Magnetoconvection and thermosolutal convection are so similar that we can be confident that the same correspondence applies here.

There are several approaches that might be followed in order to establish the overall bifurcation structure for the problem discussed here. The most straightforward procedure is to use a truncated modal expansion that describes interactions between single-roll and two-roll solutions only. The simplest consistent truncation leads to a seventeenth-order system which could be reduced to an eleventh-order system that preserves the same essential bifurcation structure (Nagata *et al.* 1990). Experience with the analogous problem in magnetoconvection reveals the shortcomings of this approach: the truncated model systems possess many irrelevant subsidiary bifurcations with unwanted solution branches which clutter up a bifurcation diagram. We prefer to be economical with our bifurcations. Then it is possible to construct a simplified bifurcation diagram that is consistent with the results obtained in numerical experiments – but this can also be done from first principles without exploring model systems. Thus the results obtained by Nagata *et al.* (1990) already indicate the form that the bifurcation structure must have here and there is no need to repeat their calculations for thermosolutal convection.

In figure 9 we have constructed a conjectural bifurcation diagram for our problem. This is an idealized pattern, with the minimum number of solution branches needed for a self-consistent picture. For simplicity we have suppressed all the bifurcations associated with transitions to chaos at heteroclinic bifurcations. Even so there are seven solution branches with eleven local and three global bifurcations. We distinguish between branches of single-roll, two-roll and mixed-mode solutions, labelled i, x and m respectively. From table 1 the pure single-roll solutions appear at lower values of R_T than the two-roll solutions. The stability properties of these branches are determined by four significant eigenvalues and the signs of the real parts of these eigenvalues are displayed in the figure, with a zero eigenvalue indicated

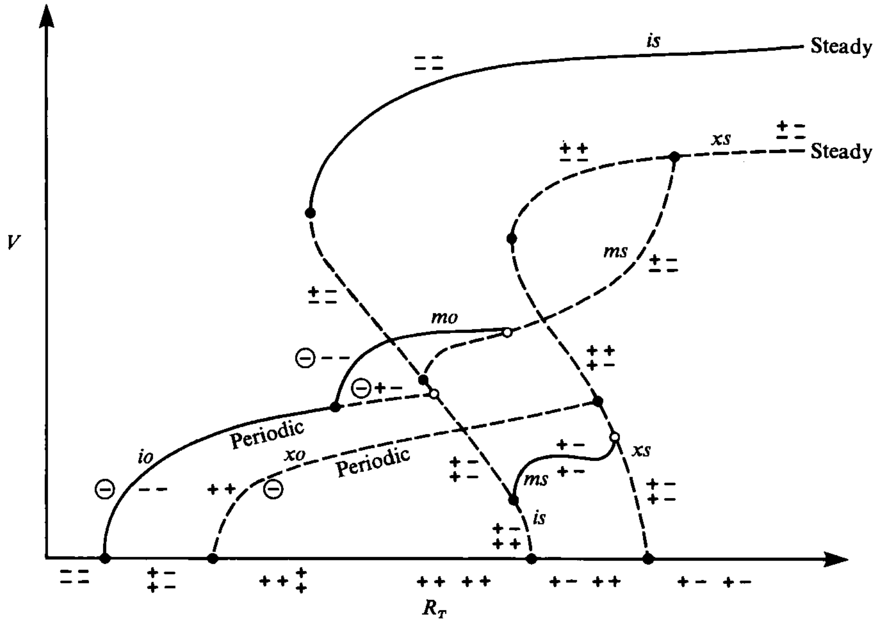

FIGURE 9. Conjectural bifurcation diagram, showing branches of steady and oscillatory pure single-roll (*is*, *io*), pure two-roll (*xs*, *xo*) and mixed-mode (*ms*, *mo*) solutions in the (R_T, V)-plane. Solid (broken) lines denote stable (unstable) solutions and local (global) bifurcations are indicated by filled (hollow) circles. The signs of the real parts of the four relevant eigenvalues are shown, with a zero eigenvalue for periodic solutions. This is a minimal bifurcation pattern and structure near the heteroclinic bifurcations is suppressed.

for periodic solutions. Stable and unstable solutions are represented by full and broken lines respectively.

We consider first pure single-roll solutions with the point symmetry i. We know that steady solutions exist for $R \geqslant R_T^{(\text{min})}$, where $R_T^{(\text{min})} < R_T^{(\text{e})}$, so the bifurcation structure is that associated with a double-zero Bogdanov bifurcation with Z_2 symmetry and the oscillatory branch terminates in a heteroclinic bifurcation on the non-stable segment of the steady branch (Knobloch & Proctor 1981; Da Costa *et al.* 1981; Coullet & Spiegel 1983; Guckenheimer & Holmes 1983; Weiss 1987). The upper pair of eigenvalues correspond to point-symmetric perturbations. Pure two-roll solutions with the symmetry m_x have a similar structure and the lower pair of eigenvalues correspond to perturbations with the same symmetry.

Next we consider the branch of oscillatory mixed-mode solutions, which bifurcates from the branch of oscillatory single-roll solutions as shown. (Although the normal form for a double Hopf bifurcation allows only quasi-periodic mixed-mode oscillations, resonant interactions lead to periodic mixed-mode oscillations in double convection.) The behaviour of solutions on this branch, summarized in figure 7, indicates that it too ends in a heteroclinic bifurcation. Hence there must be a branch of mixed-mode steady solutions with a single positive eigenvalue. This has to bifurcate from the branch of steady single-roll solutions and ends (for tidiness) on the upper part of the branch of two-roll solutions. (If it ends on the lower part there has to be a branch of periodic solutions emerging from a tertiary Hopf bifurcation and terminating in a heteroclinic bifurcation (cf. Knobloch & Moore 1990).) The signs of the eigenvalues then require for consistency that there should be a second non-stable branch of mixed-mode solutions linking the two branches of pure solutions as shown.

This minimal structure seems to be unique. It can be embellished with further branches and additional bifurcations to describe more complicated behaviour: for instance, there are resonant interactions with three-roll solutions, while the Shil'nikov mechanism involves an infinite number of bifurcations (Wiggins 1988).

There is of course a more systematic approach. Bifurcation structures like that in figure 9 can be generated analytically by constructing normal form equations that describe behaviour in the neighbourhood of a multiple bifurcation (Arnol'd 1983; Guckenheimer & Holmes 1983). For example, behaviour near a degenerate codimension-three bifurcation for pure single-roll or two-roll solutions (where $R_S = R_S^{(c)}$ and $R_T^{(o)} = R_T^{(e)}$) is described by a second-order evolution equation of the form

$$\ddot{A} + (\mu - CA^2)\dot{A} + (\nu + \kappa A^2 - EA^4)A = 0, \tag{28}$$

where C, E are constants and μ, ν, κ are parameters. With $E = 0$ this is just the Bogdanov normal form equation; the fifth-order term is added in order to represent the turning point at $R_T = R_T^{(\min)}$ (cf. Dangelmayr, Armbruster & Neveling 1985). To describe behaviour near the degenerate codimension-six bifurcation, where the single-roll and two-roll solutions all bifurcate simultaneously from the trivial solution we might construct a pair of coupled equations of the form

$$\ddot{A}_1 + (\mu_1 - C_1 A_1^2 - F_1 A_2^2)\dot{A}_1 + (\nu_1 + \kappa_1 A_1^2 + G_1 A_2^2 - E_1 A_1^4)A_1 = 0, \tag{29}$$

$$\ddot{A}_2 + (\mu_2 - C_2 A_2^2 - F_2 A_1^2)\dot{A}_2 + (\nu_2 + \kappa_2 A_2^2 + G_2 A_1^2 - E_2 A_2^4)A_2 = 0, \tag{30}$$

where C_i, E_i, F_i, G_i are constants and μ_i, ν_i, κ_i are parameters (cf. Nagata *et al.* 1990). Thermosolutal convection has a simplifying feature. The temperature and solute fields have similar structures (cf. (11) and (12)) whence it follows that the same choice of aspect ratio ($\lambda = 2.027$) guarantees that the values of $R_T^{(o)}$ and the values of $R_T^{(e)}$ are the same for single-roll and two-roll instabilities. Hence there is a double Bogdanov bifurcation, with four zero eigenvalues, at $R_S = R_S^{(c)}$. For thermosolutal convection this is actually a bifurcation of codimension three and we should set $\mu_1 = \mu_2$ in (29) and (30). We may expect the resulting system to yield a great variety of bifurcation diagrams, including one like that in figure 9. Note, however, that the relevant eigenvalues along the steady branch in (28) remain real, so any chaos in the fourth-order system will involve mixed-mode solutions only, as in the case of D_4 symmetry (Armbruster, Guckenheimer & Kim 1989). Equations (29) and (30) have not yet been studied in any detail and more work is needed in order to investigate their properties.

7. Conclusion

We have studied a specific system in some detail in order to demonstrate the interplay between physical properties of the fluid motion and constraints imposed by bifurcation theory. To describe the resulting spatiotemporal structure we have first to classify the symmetries of the system. Then we carried out a systematic numerical investigation of spatially asymmetric oscillations, following branches of stable mixed-mode solutions from the initial symmetry-breaking bifurcation to the final heteroclinic bifurcation. These new results complement and extend the survey of pure temporal behaviour by Knobloch *et al.* (1986*b*). They also show that numerical experiments cannot be adequately interpreted until the associated bifurcation structure has been understood.

Although there have been several numerical studies of spatial symmetry breaking in two-dimensional convection (Weiss 1981; Curry *et al.* 1984; Lennie *et al.* 1988; Tuckerman & Barkley 1988; Leibovich, Lele & Moroz 1989) we have succeeded in providing a more precise analysis than was hitherto available. At the same time, we have emphasized the fact that solutions found in numerical experiments depend on the symmetry constraints imposed on the model problem. As we have shown, spatially symmetric solutions become unstable when the constraint of point symmetry is relaxed. As the aspect ratio is increased more unstable modes appear, allowing richer spatiotemporal behaviour to develop (Deane, Knobloch & Toomre 1988; Moore *et al.* 1990*a*). Moreover, travelling waves are preferred to standing waves if the mirror-symmetric lateral boundary conditions (7) are replaced by periodic boundary conditions (Bretherton & Spiegel 1983; Knobloch *et al.* 1986*a*). In addition, we expect that, if three-dimensional solutions were permitted, much of the bifurcation structure described here would become unstable to three-dimensional disturbances.

The justification for studying restricted problems is that they reveal generic patterns of behaviour. Thus the spatial symmetries discussed here apply also to axisymmetric stellar dynamos (Jennings & Weiss 1991). Our real aim is to understand more complicated systems. But it is only by analysing transitions in idealized configurations that we shall eventually be able to describe the development of complicated spatiotemporal behaviour in fully three-dimensional convection.

We are grateful for discussions with Herbert Huppert, Richard Jennings, Edgar Knobloch, Michael Proctor and Juri Toomre. Computations were carried out on Cray-1S computers at ULCC. N.O.W. held a SERC Senior Fellowship while this research was carried out.

Appendix. Temporal symmetries

A dissipative system cannot have time-reversal as a symmetry, though periodic solutions may have a symmetry $t \rightarrow -t$ for suitably chosen origins in time (McKenzie 1988). For example, a Hamiltonian system described by a potential $V(a)$ such that $\ddot{a} = -\mathrm{d}V/\mathrm{d}a$ has solutions with the symmetry $m_t: (t, a) \rightarrow (-t, a)$ if $\dot{a} = 0$ at $t = 0$. Sinusoidal or snoidal oscillations possess this symmetry but it does not hold for a typical relaxation oscillation (e.g. a solution of the van der Pol equation). In thermosolutal convection such a symmetry (with suitable phase shifts) applies at the Hopf bifurcation (McKenzie 1988). In the nonlinear regime temporal symmetries correspond to those of the normal form equation for a Bogdanov bifurcation with Z_2 symmetry:

$$\ddot{a} - (\mu - a^2)\,\dot{a} + (\nu - a^2)\,a = 0 \tag{A 1}$$

(Guckenheimer & Holmes 1983). The symmetry m_t holds as an approximation in the neighbourhood of the Hopf bifurcation at $\mu = 0$ or the double bifurcation at $\mu = \nu = 0$. It is not, however, a symmetry of finite-amplitude oscillations; they are influenced by the heteroclinic bifurcation at the end of the oscillatory branch, where the orbit approaches a saddle point with real eigenvalues q, $-p$, $p > q > 0$. In fact, steady and periodic solutions of the van der Pol–Duffing equation (A 1) are described by the symmetry group D_2 with elements

$$i:\quad (t,a) \rightarrow (t, -a), \quad t_e:\quad (t,a) \rightarrow (t + \tfrac{1}{2}P, a), \quad t_i:\quad (t,a) \rightarrow (t + \tfrac{1}{2}P, -a). \tag{A 2}$$

Breaking the symmetry i of the trivial solution corresponds either to a pitchfork bifurcation, leading to steady solutions with the symmetry t_e, or to a Hopf bifurcation leading to periodic solutions with the symmetry t_i.

Period doubling can be described with the same formalism (McKenzie 1988). We consider solutions of period $2P$ with the symmetries t_P: $(t, a) \rightarrow (t+P, a)$, t_t and $t_t t_P$, which form the cyclic group Z_4, with a single invariant Z_2 subgroup $\{E, t_P\}$. This structure allows a loss of temporal symmetry (breaking t_t) followed by period doubling (breaking t_P).

REFERENCES

ARNOL'D, V. I. 1983 *Geometrical Methods in the Theory of Ordinary Differential Equations*. Springer.

ARMBRUSTER, D., GUCKENHEIMER, J. & KIM, S. 1989 Chaotic dynamics in systems with square symmetry. *Phys. Lett* A **140**, 416–420.

BRETHERTON, C. & SPIEGEL, E. A. 1983 Intermittency through modulational instability. *Phys. Lett.* A **96**, 152–156.

CASH, J. R. & MOORE, D. R. 1980 A high order method for the numerical solution of two-point boundary value problems. *BIT* **20**, 44–53.

COULLET, P. H. & SPIEGEL, E. A. 1983 Amplitude equations for systems with competing instabilities. *SIAM J. Appl. Maths.* **43**, 776–821.

CURRY, J. H., HERRING, J. R., LONCARIC, J. & ORSZAG, S. A. 1984 Order and disorder in two- and three-dimensional Bénard convection. *J. Fluid Mech.* **147**, 1–38.

DA COSTA, L. N., KNOBLOCH, E. & WEISS, N. O. 1981 Oscillations in double-diffusive convection. *J. Fluid Mech.* **109**, 25–43.

DANGELMAYR, G., ARMBRUSTER, D. & NEVELING, M. 1985 A codimension three bifurcation for the laser with saturable absorber. *Z. Phys.* B **59**, 365–370.

DEANE, A. E., KNOBLOCH, E. & TOOMRE, J. 1988 Travelling waves in large-aspect ratio thermosolutal convection. *Phys. Rev.* A **37**, 1817–1820.

GOLDHIRSCH, I., PELZ, R. B. & ORSZAG, S. A. 1989 Numerical simulation of thermal convection in a two-dimensional finite box. *J. Fluid Mech.* **199**, 1–28.

GOLUBITSKY, M. & SCHAEFFER, D. 1985 *Singularities and Groups in Bifurcation Theory*. Springer.

GUCKENHEIMER, J. & HOLMES, P. 1983 *Nonlinear Oscillations, Dynamical Systems and Bifurcations of Vector Fields*. Springer.

HUPPERT, H. E. & MOORE, D. R. 1976 Nonlinear double-diffusive convection. *J. Fluid Mech.* **78**, 821–854.

JENNINGS, R. L. & WEISS, N. O. 1991 Symmetry breaking in stellar dynamos. *Mon. Not. R. Astron. Soc.* (in press).

JOSEPH, D. D. 1976 *Stability of Fluid Motions II*. Springer.

KNOBLOCH, E., DEANE, A. E., TOOMRE, J. & MOORE, D. R. 1986*a* Doubly diffusive waves. *Contemp. Maths* **56**, 203–216.

KNOBLOCH, E. & MOORE, D. R. 1990 Minimal model of binary fluid convection. *Phys. Rev.* A **42**, 4693–4709.

KNOBLOCH, E., MOORE, D. R., TOOMRE, J. & WEISS, N. O. 1986*b* Transitions to chaos in two-dimensional double-diffusive convection. *J. Fluid Mech.* **166**, 409–448 (referred to herein as I).

KNOBLOCH, E. & PROCTOR, M. R. E. 1981 Nonlinear periodic convection in double-diffusive systems. *J. Fluid Mech.* **108**, 291–316.

LEIBOVICH, S., LELE, S. K. & MOROZ, I. 1989 Nonlinear dynamics in Langmuir circulations and in thermosolutal convection. *J. Fluid Mech.* **198**, 471–511.

LENNIE, T. B., MCKENZIE, D. P., MOORE, D. R. & WEISS, N. O. 1988 The breakdown of steady convection. *J. Fluid Mech.* **188**, 47–85.

MCKENZIE, D. P. 1988 The symmetry of convection transitions in space and time. *J. Fluid Mech.* **191**, 287–339.

MOORE, D. R., PECKOVER, R. S. & WEISS, N. O. 1973 Difference methods for time-dependent two-dimensional convection. *Comput. Phys. Commun.* **6**, 198–220.

MOORE, D. R., TOOMRE, J., KNOBLOCH, E. & WEISS, N. O. 1983 Period-doubling and chaos in partial differential equations for thermosolutal convection. *Nature* **303**, 663–667.

MOORE, D. R. & WEISS, N. O. 1990 Dynamics of double convection. *Phil. Trans. R. Soc. Lond.* A **332**, 121–134.

MOORE, D. R., WEISS, N. O. & WILKINS, J. M. 1990*a* Symmetry-breaking in thermosolutal convection. *Phys. Lett.* A **147**, 209–214.

MOORE, D. R., WEISS, N. O. & WILKINS, J. M. 1990*b* The reliability of numerical experiments: transitions to chaos in thermosolutal convection. *Nonlinearity* **3**, 997–1014.

NAGATA, M., PROCTOR, M. R. E. & WEISS, N. O. 1990 Transactions to asymmetry in magnetoconvection. *Geophys. Astrophys. Fluid Dyn.* **51**, 211–241.

PROCTOR, M. R. E. & WEISS, N. O. 1982 Magnetoconvection. *Rep. Prog. Phys.* **45**, 1317–1379.

PROCTOR, M. R. E. & WEISS, N. O. 1990 Normal forms and chaos in thermosolutal convection. *Nonlinearity* **3**, 619–637.

SATTINGER, D. H. 1978 Group representation theory, bifurcation theory and pattern formation. *J. Funct. Anal.* **28**, 58–101.

SHI, A. & ORSZAG, S. A. 1987 Order and disorder in two-dimensional double-diffusive convection. Preprint.

TUCKERMAN, L. S. & BARKLEY, D. 1988 Global bifurcations to traveling waves in axisymmetric convection. *Phys. Rev. Lett.* **61**, 408–411.

VERONIS, G. 1968 Effect of a stabilizing gradient of solute on thermal convection. *J. Fluid Mech.* **34**, 315–336.

WEISS, N. O. 1981 Convection in an imposed magnetic field Part 2. The dynamical regime. *J. Fluid Mech.* **108**, 273–289.

WEISS, N. O. 1987 Dynamics of convection. *Proc. R. Soc. Lond.* A **413**, 71–85.

WEISS, N. O. 1990 Symmetry breaking in nonlinear convection. In *Nonlinear Evolution of Spatio-temporal Structures in Dissipative Continuous Systems* (ed. F. Busse & L. Kramers), pp. 359–374. Plenum.

WIGGINS, S. 1988 *Global Bifurcations and Chaos*. Springer.